LA-UR- 09-00588

Approved for public release;
distribution is unlimited.

Title:	Pore scale modeling of reactive transport involved in geologic CO2 sequestration
Author(s):	Qinjun Kang Peter Lichtner Hari Viswanathan Amr Abdel-Fattah
Intended for:	Publication in Transport in Porous Media

Los Alamos
NATIONAL LABORATORY
EST.1943

Form 836 (7/06)

Noname manuscript No.
(will be inserted by the editor)

Pore scale modeling of reactive transport involved in geologic CO_2 sequestration

Qinjun Kang · Peter C. Lichtner · Hari S. Viswanathan · Amr I. Abdel-Fattah

Received: date / Accepted: date

Abstract We apply a multi-component reactive transport lattice Boltzmann model developed in previous studies to modeling the injection of a CO_2 saturated brine into various porous media structures at temperature T=25 and 80°C. The porous media are originally consisted of calcite. A chemical system consisting of Na^+, Ca^{2+}, Mg^{2+}, H^+, $CO_2^o(aq)$, and Cl^- is considered. The fluid flow, advection and diffusion of aqueous species, homogeneous reactions occurring in the bulk fluid, as well as the dissolution of calcite and precipitation of dolomite are simulated at the pore scale. The effects of porous media structure on reactive transport are investigated. The results are compared with continuum scale modeling and the agreement and discrepancy are discussed. This work may shed some light on the fundamental physics occurring at the pore scale for reactive transport involved in geologic CO_2 sequestration.

1 Introduction

Disposal of CO_2 in geologic formations represents one of the most promising near-term solutions to the problem of reducing carbon emissions into the atmosphere [1]. Still, the public must be assured by convincing scientific research that CO_2 may be safely injected and sequestered. As predictive models are utilized to assess the impact of CO_2 injection on the subsurface, these simulators must account for multiple physiochemical processes involving interactions between the injected CO_2, the brine in the pore spaces, and the minerals lining the pores. For example, injection of CO_2 into limestone formations may increase the permeability of the rock near the wellbore through processes such as wormholing, while precipitation of carbonate minerals may reduce permeability, as a result of pH increases caused by reaction with the host rock. All these processes are ultimately governed by pore-scale interfacial phenomena, which occur at scales of microns. However, because of the wide disparity in scales ranging from pore to field, it is virtually impossible to solve the pore-scale governing equations

Q. Kang
Computational Earth Science Group (EES-16), Los Alamos National Laboratory
Tel.: +1-505-6659663
Fax: +1-505-6658737
E-mail: qkang@lanl.gov

at the field scale. Instead, in modeling geologic CO_2 sequestration, a continuum formulation based on spatial averages taken over length scales much larger than typical pore and mineral grain sizes is often utilized, implying the existence of a representative elemental volume (REV) [2]. As a result, spatial heterogeneities at smaller scales are unresolved and the aggregate effect of the porescale processes are taken into account through various effective constitutive parameters such as permeability, dispersivity, tortuosity, and specific mineral surface area. One of the goals of performing pore-scale simulations is to obtain values for these constitutive parameters through upscaling the pore-scale results. Other goals are to identify key parameters and physiochemical processes that control macroscopic phenomena, to validate continuum descriptions, and to determine the most appropriate form of the continuum formulation (single, dual, multiple continua) that can best approximate the pore-scale results [3].

Because of its importance, the general problem of reactive transport at the pore scale has been studied extensively using various approaches under different simplifying conditions [4–17]. However, only recently has the full complexity of the strongly coupled flow, transport, and precipitation/dissolution reactions in realistic geochemical systems been considered [18–21].

Recently, Kang et al. [18, 19] developed a lattice Boltzmann (LB) pore-scale model for simulating reactive transport in systems with multiple aqueous components and minerals. This model takes into account advection, diffusion, homogeneous reactions among multiple aqueous species, heterogeneous reactions between the aqueous solution and minerals, as well as the resulting geometrical changes in pore space. In this contribution, this model will be applied to modeling injection of a CO_2 saturated brine solution into various porous media structures originally consisted of calcite. The dissolution of calcite and precipitation of dolomite will be simulated and the effects of the porous media structure on reactive transport will be investigated.

2 Numerical Methods

For completeness, we first briefly present the pore-scale LB model for multicomponent reactive transport in porous media developed in previous studies. We also describe enhancements to the model since then. Interested readers may refer to [18, 19] for more details.

2.1 Incompressible lattice Boltzmann model for fluid flow

It is well known that the conventional LB method actually solves the compressible pore-scale Navier-Stokes (NS) equations in the nearly incompressible limit with an equation of state representing an ideal gas law. The density variation and Mach number of the fluid must be very small for an accurate simulation of incompressible flows. These requirements, especially small density variations, limit the applicability of conventional LB models for practical problems involving flow through porous media, because in these problems, fluid motion is often driven by large pressure gradients, or, equivalently, elevated density gradients. For low permeable media, even if the pore velocity (Mach number) is small, the pressure (density) gradient can be very large. Therefore, use of the conventional LB model to simulate flow in porous media may introduce significant density changes (and hence compressibility error). Furthermore, when the velocity field

obtained from the conventional LB model is applied to solute transport simulation, one may obtain an unphysical breakthrough curve (breakthrough too early) for a tracer, or worse, an unphysical disequilibrium of an otherwise chemically equilibrated system for reactive solutes [3].

To eliminate these compressible effects, here we use an incompressible LB model constructed by Guo et al. [22]. The pore-scale flow of a single aqueous fluid phase is simulated by the following evolution equation:

$$f_\alpha(\mathbf{x}+\mathbf{e}_\alpha\delta t, t+\delta t) = f_\alpha(\mathbf{x},t) - \frac{f_\alpha(\mathbf{x},t) - f_\alpha^{\mathrm{eq}}(\mathbf{x},t)}{\tau}. \tag{1}$$

In the above equation, δt is the time increment, f_α the distribution function along the α direction in velocity space, f_α^{eq} the corresponding equilibrium distribution function, and τ the dimensionless relaxation time. For the commonly used two-dimensional, nine-speed LB model (D2Q9), as shown in figure 1 the discrete velocities $\mathbf{e}_\alpha$ have the following form:

$$\mathbf{e}_\alpha = \begin{cases} 0, & (\alpha=0), \\ (cos\frac{(\alpha-1)\pi}{2}, sin\frac{(\alpha-1)\pi}{2})c, & (\alpha=1-4), \\ \sqrt{2}(cos[\frac{(\alpha-5)\pi}{2}+\frac{\pi}{4}], sin[\frac{(\alpha-5)\pi}{2}+\frac{\pi}{4}])c, & (\alpha=5-8). \end{cases} \tag{2}$$

For the incompressible LB model, the equilibrium distribution is defined by Guo et al. [22]:

$$f_\alpha^{eq} = \begin{cases} -4\sigma\frac{p}{\rho c^2} + s_\alpha(\mathbf{u}), & (\alpha=0), \\ \lambda\frac{p}{\rho c^2} + s_\alpha(\mathbf{u}), & (\alpha=1-4), \\ \gamma\frac{p}{\rho c^2} + s_\alpha(\mathbf{u}), & (\alpha=5-8), \end{cases} \tag{3}$$

where σ, λ, and γ are parameters satisfying

$$\lambda + \gamma = \sigma$$

$$\lambda + 2\gamma = \frac{1}{2},$$

and

$$s_\alpha(\mathbf{u}) = \omega_\alpha\left[\frac{3\mathbf{e}_\alpha\cdot\mathbf{u}}{c^2} + \frac{9(\mathbf{e}_\alpha\cdot\mathbf{u})^2}{2c^4} - \frac{3\mathbf{u}\cdot\mathbf{u}}{2c^2}\right]. \tag{4}$$

In these equations, $c = \delta x/\delta t$, where δx is the space increment, and p and $\mathbf{u}$ are the pressure and velocity of the fluid, respectively. The corresponding weight coefficients are $\omega_0 = 4/9$, $\omega_\alpha = 1/9$ for $\alpha = 1,2,3,4$, and $\omega_\alpha = 1/36$ for $\alpha = 5,6,7,8$.

Equation (3) has been shown to recover the following incompressible NS equations [22]:

$$\nabla\cdot\mathbf{u} = 0, \tag{5}$$

$$\frac{\partial\mathbf{u}}{\partial t} + \nabla\cdot(\mathbf{uu}) = -\frac{1}{\rho}\nabla p + \nu\nabla^2\mathbf{u}, \tag{6}$$

with the velocity and pressure given by

$$\mathbf{u} = \sum_{\alpha=1}^{8}\mathbf{e}_\alpha f_\alpha, \tag{7}$$

and

$$\frac{p}{\rho} = \frac{c^2}{4\sigma}\left[\sum_{\alpha=1}^{8} f_\alpha + s_0(\mathbf{u})\right], \tag{8}$$

and the viscosity is determined by

$$\nu = \frac{(\tau - 1/2)(\delta x)^2}{3\delta t}, \tag{9}$$

2.2 Homogeneous reactions in the bulk fluid

In a previous paper, Kang et al. [18] have derived the following LB equation for the total primary species concentrations for chemical systems with reactions written in canonical form:

$$G_{\alpha j}(\mathbf{x} + \mathbf{e}_\alpha \delta t, t + \delta t) = G_{\alpha j}(\mathbf{x}, t) - \frac{G_{\alpha j}(\mathbf{x}, t) - G^{\mathrm{eq}}_{\alpha j}(\Psi_j, \mathbf{u})}{\tau_{\mathrm{aq}}}, \quad (j = 1, \cdots, N_C), \tag{10}$$

where N_C is the number of primary species, Ψ_j is the total concentration of the jth primary species, $G_{\alpha j}$ is its distribution function along the α direction, $G^{\mathrm{eq}}_{\alpha j}$ is the corresponding equilibrium distribution function, $\mathbf{e}_\alpha$ are velocity vectors, δt is the time increment, and τ_{aq} is the dimensionless relaxation time. Here we use D2Q4 model for solute transport, as it has been shown to have comparable accuracy with the D2Q9 model but better computational efficiency [19]. The equilibrium distribution takes the following linear form:

$$G^{\mathrm{eq}}_{\alpha j} = \frac{\Psi_j}{4} + \frac{\Psi_j}{2c^2}(\mathbf{e}_\alpha \cdot \mathbf{u}). \tag{11}$$

with

$$\mathbf{e}_\alpha = (cos\frac{(\alpha-1)\pi}{2}, sin\frac{(\alpha-1)\pi}{2})c, (\alpha = 1 - 4). \tag{12}$$

Noble [23] has shown that equation (10) can recover the following pore-scale advection-diffusion equation for Ψ_j:

$$\frac{\partial \Psi_j}{\partial t} + \nabla \cdot \mathbf{\Omega}_j = 0, \tag{13}$$

with

$$\Psi_j = \sum_\alpha G_{\alpha j}, \tag{14}$$

and

$$\mathbf{\Omega}_j = \mathbf{u}\Psi_j - \mathcal{D}\nabla\Psi_j, \tag{15}$$

as the flux of the total concentration of the jth primary species due to both advection and diffusion. The diffusivity is given by

$$\mathcal{D} = \frac{(\tau_{\mathrm{aq}} - 1/2)(\delta x)^2}{2\delta t}. \tag{16}$$

Assuming the homogeneous reactions are in instantaneous equilibrium, we have the following mass action equations [24,25]:

$$C_i = (\gamma_i)^{-1} K_i \prod_{j=1}^{N_C} (\gamma_j C_j)^{\nu_{ji}}, \tag{17}$$

where ν_{ji} are the stoichiometric coefficients, K_i is the equilibrium constant of the ith homogeneous reaction, γ_i is the activity coefficient of the ith secondary species, and C_j and C_i are solute concentrations for primary and secondary species, respectively. They are related to Ψ_j by

$$\Psi_j = C_j + \sum_{i=1}^{N_R} \nu_{ji} C_i, \tag{18}$$

where N_R is the number of independent homogeneous reactions, or, equivalently, secondary species.

2.3 Heterogeneous reactions at mineral interfaces

Heterogeneous reactions taking place at mineral interfaces are incorporated through boundary conditions. The following boundary condition for the total concentrations Ψ_j has been employed in the paper by Kang et al. [18]:

$$\mathcal{D}\frac{\partial \Psi_j}{\partial n} = -\sum_{m=1}^{N_m} \nu_{jm} k_m \left(1 - K_m Q_m\right). \tag{19}$$

In this equation, n is the direction normal to the interface pointing toward the fluid phase, k_m is the reaction rate constant, K_m is the equilibrium constant, and the ion activity product Q_m is defined by

$$Q_m = \prod_{j=1}^{N_C} (\gamma_j C_j)^{\nu_{jm}}. \tag{20}$$

In this study, we use the improved LB implementation of the above boundary condition, which strictly conserves mass during the heterogeneous reactions [19]. The formulation of the unknown distribution functions at the fluid/solid interface depends on the orientation of the surface. For a wall node shown in Figure 2, the unknown distribution function G_{2j} can be calculated by:

$$G_{2j} = \Psi_j/2 - G_{4j}, \tag{21}$$

where Ψ_j is determined from equation (18) after C_j is calculated from the following nonlinear algebraic equation through Newton-Raphson iteration method:

$$2G_{4j} = \frac{\Psi_j}{2} - \frac{1}{c}\sum_{m=1}^{N_m} \nu_{jm} k_m \left(1 - K_m Q_m\right). \tag{22}$$

2.4 Update of solid phase

Since the solid movement with fluid flow is not considered, the volume of the stationary solids satisfies the following equation:

$$\frac{\partial V_m}{\partial t} = \overline{V}_m a_m I_m^*, \tag{23}$$

where V_m, $\overline{V}_m$, and a_m are dimensionless volume, molar volume, and specific surface area of the mth mineral, respectively. Solute diffusion in the solid phase is neglected and mineral reactions are assumed to only occur at the fluid-solid interface. Each interface node represents a control volume (a control area in the 2D case) with a size of 1×1 (in lattice units) and is located at the center of this volume. As can be seen from figure 2, node Q is the center of the control volume surrounded by dashed lines. The initial control volume is given a dimensionless volume V_m^0. The volume is updated at each time step explicitly according to the equation

$$V_m(t + \delta t) = V_m(t) + \overline{V}_m a_m I_m^* \delta t, \tag{24}$$

where δt is the time increment. In this study both δt and a_m equal unity in lattice units.

When V_m reaches certain threshold values, the pore geometry needs to be updated. For dissolution, the solid node associated with V_m can be simply removed (i.e., changed to a pore node), when V_m reaches zero. For precipitation, however, there are multiple ways to add a solid node when V_m reaches a certain threshold value. A random-growth method was proposed by Kang et al. for single-species [16] and multi-component systems [18]. In that method, the growth has no preference in any particular direction and the method has been shown to be lattice-effect free. Growth in preferred directions can be achieved by incorporating corresponding physics in the growth rules. For example, polygonal and dendritic crystals with symmetry have been produced by aligning the direction of growth to that of the maximum concentration gradient and different morphologies have been obtained by varying the probability of adding a solid node in that direction [26].

In the above methods, the grid size is assumed to be small enough that each node is only represented by one mineral at one time, and the effect of both dissolution and precipitation is recorded at that node through equation (24). In reality, changes of solid morphology can involve scales much smaller than the lattice or pore size used in the simulations. In this study, we assume that each node can be represented by multiple minerals whose initial total volume fraction amounts to unity. The volume fraction of each mineral is still updated by equation (24) and dissolution recorded in the solid node. Mass accumulation due to precipitation, however, is recorded at the neighboring pore nodes. As seen in figure 2, when

$$\sum_m V_m(Q) = 0, \tag{25}$$

node Q is changed to a fluid node. When

$$\sum_m V_m(S) = 1, \tag{26}$$

node S becomes a solid node consisted of multiple minerals. In contrast to previous methods [16, 18] for updating pore geometry, the current method can account for coexistence of multiple minerals at the same node and the growth is deterministic rather than random. However, the underlying physical properties/processes associated with various growth methods are not clear and need to be identified through high resolution microscopic experiments.

3 Simulation Examples

3.1 Porous media structures

Fig. 3 shows porous media structures used in the simulations. They are periodic array of small circles (geo1), large circles (geo2), horizontal ellipses (geo3), and vertical ellipses (geo4), respectively. Table 1 lists the properties of the four porous media, including particle size, porosity, and permeability. The size (area) of the small circle is the same as that of the horizontal or vertical ellipse, while that of the large circle is three times greater. The specific surface area of the ellipses is slightly higher than that of the small circle, while the large circle has the smallest specific surface area. Particle size and porosity are prescribed when the images are generated, and permeability is calculated using the incompressible LB model presented here. The same structures have been used in [27] to investigate the effects of porous media geometry on a transverse mixing-limited chemical reaction. Unlike the micromixing problem, in our study, the structure is periodic in the y direction. Therefore, we can use only one REV in that direction and a relative long domain in the main flow direction. Figure 4 shows an REV for the small circle porous structure, with a size of 48×48. Hence the grid size is 1728×48, 1728×96, 1728×36, and 1728×64 for the four porous media, respectively. The grid resolution is 1×10^{-5} m (10 microns).

3.2 Chemical system and reaction kinetics

The chemical system in the aqueous phase can be described by six components: Na^+, Ca^{2+}, Mg^{2+}, H^+, $CO_2^\circ(aq)$, and Cl^-, and a number of complexes (secondary species) of varying importance: OH^-, CO_3^{2-}, HCO_3^-, $CaCO_3^\circ$, $CaHCO_3^+$, $CaOH^+$, $MgCO_3^\circ$, $MgHCO_3^+$, $MgOH^+$, $NaCl^\circ$, $NaHCO_3^\circ$, and $NaOH^\circ$.

Calcite According to Chou et al. [28] the calcite rate law has the form

$$R = -\left(k_1 a_{H^+} + k_2 a_{H_2CO_3(aq)} + k_3\right)\left[1 - K_{CC} Q_{CC}\right], \tag{27}$$

where k_1, k_2, and k_3 are the reaction rate constants, a_{H^+} and $a_{H_2CO_3}(\mathrm{aq})$ refer to the activities of H^+ and HCO_3^-, respectively, K_{CC} is the equilibrium constant, and Q_{CC} the ion activity product. The values of k_1, k_2, and k_3 at 25°C are 0.89×10^{-4}, 5.01×10^{-8}, and 6.6×10^{-11} mol cm^{-2}s^{-1}, respectively. The calcite reaction rate is pH-dependent under acidic conditions and becomes almost constant above a pH of about 7.

Dolomite According to Gautelier et al. [29] the dolomite rate in the pH range 0.5-5 is given by

$$R = -k a_{H^+}^n \left(1 - K_{dol} Q_{dol}\right). \tag{28}$$

Values for k and n are listed in Table 2.

Temperature dependence The temperature dependence of the kinetic rate constants is given by the Arrhenius expression

$$k(T) = k_0 \exp\left[-\frac{\Delta E}{R}\left(\frac{1}{T} - \frac{1}{T_0}\right)\right], \tag{29}$$

where k_0 denotes the rate constant at the reference temperature T_0, usually taken to be 25°C, R denotes the gas constant, and ΔE the mineral activation energy.

By comparison, the diffusion coefficient depends on temperature according to the relation:

$$D(T) = D_0 \exp\left[-\frac{\Delta E_D}{R}\left(\frac{1}{T} - \frac{1}{T_0}\right)\right]. \tag{30}$$

Clearly, both the reaction rate constants and diffusion coefficient increase with temperature. Two temperature points (T =25°C and 80°C) are considered in this study. T =80°C is probably more close to the working environment of geologic CO_2 sequestration. The rate constants (k_1, k_2, and k_3) for calcite at this temperature are calculated through equation (29) based on their values at 25°C and ΔE =35 kJ/mol. The diffusion coefficient of all aqueous species is assumed to be 1×10^{-9}m^2/s at 25°C and its value at 80°C is calculated using equation (30) with ΔE_D=14 kJ/mol. The equilibrium constants for different temperature points are read in from an existing database.

3.3 Boundary and initial conditions

A constant pressure gradient is imposed across the domain to establish a steady state flow field. The pressure is prescribed such that the steady-state flux for all the four initial porous media are the same (168.27 m/year). For such a long domain, the conventional LB model will result in a velocity field whose mean velocity increases along the x direction due to its inherent compressibility. The incompressible LB model presented here, however, is free of such a problem and will provide a velocity field with constant mean velocity.

The initial fluid is 2.69 M NaCl brine with pH of 7.75, in equilibrium with minerals calcite and dolomite. The initial composition of the grains is calcite. When flow reaches steady state, a fluid of pH 3.87 in equilibrium with 179 bars CO_2(g) and dolomite is injected from the left. Because of the injection of a solution with lower pH and higher CO_2 concentration, calcite dissolves, causing oversaturation of dolomite, and hence its precipitation. Zero gradient boundary conditions are imposed at the outlet for solute concentration.

3.4 Simulation results

Fig. 5 shows steady-state stream lines and contours of vertical velocity predicted by the LB model for the vertical ellipse porous medium. It is clear that the pore velocity is fully resolved. Other simulation results are shown in Figures 6 through 13.

Figures 6 and 7 show distribution of volume-averaged (over an REV) volume fraction of calcite and dolomite along the x-direction at time t=9500 seconds for all the four porous structures, and for temperature T=25°C and 80°C, respectively. For all the cases, the volume fraction of calcite decreases from its initial value (0.58) due to

dissolution while that of dolomite increases from its initial value (0) due to precipitation. The symbols of calcite and dolomite seem to be symmetric, meaning that the calcite dissolution and dolomite precipitation are complementary. Wherever calcite dissolves most, dolomite precipitates most. Unlike continuum scale model, here the volume fraction of calcite never reduces to zero, because of the armoring effect considered in the pore scale modeling. The precipitation of dolomite on top of the dissolving calcite may block the passage for the aqueous species to access the calcite, halting its further dissolution.

While the volume fraction varies smoothly along the x direction for T=25°C, it has a jump at some point for T=80°C, downstream from which the calcite is unreacted. There exists a sharp interface (reaction front) when the temperature is high (or equivalently, the reactions are fast). The reaction front of the large circle structure propagates much further than that of the other three porous media, and the mineral volume fraction for the horizontal ellipse structure almost coincides with that for the vertical ellipse structure. These results are quite different from those of the micromixing problem [27], where product formation is almost identical for small and large circles, but very different for the two ellipse structures. There are three reasons for this difference: first, the chemical reaction considered is different, while a homogeneous reaction assumed to be instantaneous is considered in the micromixing problem, in the present study, we are concerned about the heterogeneous reactions between the solution and minerals, which is treated kinetically. Second, in the former problem, the interfacial contact area between reactive species plumes is a controlling factor for mixing and extent of chemical reaction. The porous media structure only affects the process by influencing the contact between the two reacting fluids. In the latter problem, however, the reactions occur between the solution and minerals that make up the porous media. Therefore, the interfacial contact area between the solution and the minerals is a controlling factor, and specific surface area plays an important role. Third, in the former problem, the two reacting fluids are injected from the top and bottom of the structure, respectively, while in the latter problem, the transverse direction is periodic and there is no concentration gradient in that direction at the REV scale.

Figure 8 shows volume fraction for the large circle and horizontal ellipse structures at T=80°C and t=7000, 9500, and 12000 seconds. For both structures, the reaction front moves at an approximately constant velocity. Clearly, the front of the large circle structure propagates faster ($\approx$ 40 m/year) than that of the horizontal ellipse structure ($\approx$ 20 m/year). Roughly the front velocity is inversely proportional to the volume of reactive calcite ($0.58 - 0.53 = 0.05$ versus $0.58 - 0.47 = 0.11$). This is consistent with the conclusion from the continuum scale model [30]. However, the front velocity is also roughly inversely proportional to the specific surface area (6.9 versus 15.2 as shown in Table 1). This finding contradicts the continuum scale model, in which the front velocity is independent of surface area [30]. This discrepancy may be due to the armoring effect that is explicitly accounted for in the pore scale modeling. Interestingly, the ratio of the volume fraction of reactive calcite equals that of the specific surface area (both 0.45:1). However, since the armoring effect in the current method may depend on the specific way to update the solid phase, how accurate this finding is needs further scrutiny.

Continuum scale modeling using the computer code FLOTRAN [31] is also performed for horizontal ellipse structure at temperature=80°C. Two sets of calculations are shown in figure 9 for the volume fractions of calcite and dolomite: one assumes all calcite (58%) is reactive, and the other only 11% of the calcite is reactive, corresponding to the LB simulation caused by armoring of the calcite surface. In the case with all

calcite reactive the reaction front advances more slowly compared to the LB simulation, and in the other case more rapidly. It is possible to fit the front position by varing the volume fraction of reactive calcite. However, it is not possible to fit both of them simultaneously. The reason may be that in the LB simulation, the calcite surface is covered by dolomite gradually. This process is simulated in the continuum scale model by using a constant value for the volume fraction of the reactive calcite derived from the LB simulation at a longer time. The use of this single constant may be insufficient to capture the dynamic process of armoring.

Figures 10 and 11 show spacial distribution of volume fraction and reaction rate of calcite and dolomite for the small circle structure at t=9500 seconds, for T=25°C and 80°C, respectively. Only part of the domain is shown for better visualization. The dissolution of calcite and precipitation of dolomite can be seen clearly. For both temperature points, the dolomite reaction rate is always positive, meaning that dolomite only precipitates. The calcite reaction rate, however, can be either positive or negative, indicating reprecipitation of calcite.

For T=25°C, there is non-zero reaction rate for both calcite and dolomite at the surface of the circles throughout the domain. For T=80°C, however, the rate at the upstream of the reaction front is zero. This is consistent with the concentration contours shown in figures 12 and 13. Clearly there is spacial variation in the concentration of aqueous species for the lower temperature. But the concentration is almost uniform at the upstream of the reaction front for the high temperature case.

4 Conclusions

We applied a multi-component reactive transport LB model developed in previous studies to modeling the injection of a CO_2 saturated brine solution into various porous media structures at temperature T=25 and 80°C. The porous media were originally consisted of calcite. A chemical system consisting of Na^+, Ca^{2+}, Mg^{2+}, H^+, $CO_2^\circ(aq)$, and Cl^- was considered, with calcite dissolution and dolomite precipitation. It is shown that the LB model is able to provide detailed information on fluid velocity, solute concentration, mineral composition and reaction rates, as well as the evolution of the porous media geometry. It is found that for the higher temperature, there is a sharp reaction front, downstream from which the minerals are unreacted, and upstream from which the reaction rates reduce to zero. The front moves at an approximately constant velocity independent of surface area, and the velocity is roughly inversely proportional to the volume fraction of the reactive calcite, consistent with the continuum scale model. However, the front velocity is also found to be roughly inversely proportional to the specific surface, contradicting the continuum scale model. For both T=25 and 80°C, dolomite only precipitates but calcite dissolves and reprecipitates. The grain orientation has little effect on the reactive transport at the REV scale. The numerical results presented here are still subject to confirmation by high resolution microscopic experiments. Nevertheless, the results presented may help understand the fundamental physicochemical processes during CO_2 sequestration in geologic formations. A three-dimensional multi-phase multi-component model is under development and the results will be presented in future publications.

Acknowledgements This material is based upon work supported by the National Science Foundation under Grant No. CHE-0431328 and the U.S. Department of Energy, Biological

and Environmental Research (BER), by LDRD project 20070267ER sponsored by Los Alamos National Laboratory, and by Energy Zero Emission Research and Technology sponsored by the U. S. Department of Energy.

References

1. Pacala, S. and Socolow, R., Stabilization wedges: Solving the climate problem for the next 50 years with current technologies, *Science, 305,* 968-972, 2004.
2. Bear, J., *Dynamics of Fluids in Porous Media,* Elsevier, New York, 1972.
3. Lichtner, P. C., and Q. Kang, Upscaling pore-scale reactive transport equations using a multi-scale continuum formulation, *Water Resour. Res., 43,* W12S15, doi:10.1029/2006WR005664, 2007.
4. Daccord, G., Chemical dissolution of a porous medium by a reactive fluid, *Phys. Rev. Lett., 58,* 479-482, 1987.
5. Dijk, P., and B. Berkowitz, Precipitation and dissolution of reactive solutes in fracture, *Water Resour. Res., 34,* 457-470, 1998.
6. Hoefner, M. L., and H. S. Fogler, Pore evolution and channel formation during flow and reaction in porous media, *AIChE J., 34,* 45-54, 1988.
7. Wells, J. T., D. R.Janecky, and B. J. Travis, A lattice gas automata model for heterogeneous chemical-reactions at mineral surfaces and in pore networks, *Physica D, 47,* 115-123, 1991.
8. Janecky, D. R., S. Chen, and S. Dawson, et al., Lattice gas automata for flow and transport in geochemical systems, In Proceeding, 7th Int. Symp. on Water-Rock Interaction. Y.K. Kharaka and A.S. Maest(Eds), A.A. Balkema, Rotterdam, Netherlands, 1043, 1992.
9. Salles, J., J. F. Thovert, and P. M. Adler, Deposition in porous media and clogging, *Chem. Eng. Sci., 48,* 2839-2858, 1993.
10. Kelemen, P. B., J. A. Whitehead, E. Aharonov, and K. A. Jordahl, Experiments on flow focusing in soluble porous media, with applications to melt extraction from the mantle, *J. Geophys. Res., 100,* 475-496, 1995.
11. Bekri, S., J. F. Thovert, and P. M. Adler, Dissolution of porous media, *Chem. Eng. Sci., 50,* 2765-2791, 1995.
12. Bekri, S., J. F. Thovert, and P. M. Adler, Dissolution and deposition in fractures, *Eng. Geology, 48,* 283-308, 1997.
13. Fredd, C. N., and H. S. Fogler, Influence of transport and reaction on wormhole formation in porous media, *AIChE J., 44,* 1933-1949, 1998.
14. Kang, Q., D. Zhang, S. Chen, and X. He, Lattice Boltzmann simulation of chemical dissolution in porous media, *Phys. Rev. E, 65,* 036318, 2002.
15. Kang, Q., D. Zhang, and S. Chen, Simulation of dissolution and precipitation in porous media, *J. Geophy. Res., 108,* 2505, 2003.
16. Kang, Q., D. Zhang, P. C. Lichtner, and I. N. Tsimpanogiannis, Lattice Boltzmann model for crystal growth from supersaturated solution, *Geophys. Rev. Lett., 31,* L21604, 2004.
17. Kang, Q., I. N. Tsimpanogiannis, D. Zhang, and P. C. Lichtner, Numerical modeling of pore-scale phenomena during CO2 sequestration in oceanic sediments, *Fuel Proce. Tech., 86,* 1647, 2005.
18. Kang, Q., P. C. Lichtner, and D. Zhang, Lattice Boltzmann pore-scale model for multicomponent reactive transport in porous media, *J. Geophy. Res., 111,* B05203, doi:10.1029/2005JB003951, 2006.
19. Kang, Q., P. C. Lichtner, and D. Zhang, An improved lattice Boltzmann model for multicomponent reactive transport in porous media at the pore scale, *Water Resour. Res., 43,* W12S14, doi:10.1029/2006WR005551
20. Li, L., Peters C. A., Celia M. A., Upscaling geochemical reaction rates using pore-scale network modeling, *Adv. in Water Res., 29,* 13511370, 2006.
21. Tartakovsky, A. M., Meakin P., Scheibe T. D., and Wood B. D., 2007, A smoothed particle hydrodynamics model for reactive transport and mineral precipitation in porous and fractured porous media, *Water Res. Res., 43,* W05437, doi:10.1029/2005WR004770.
22. Guo, Z., B. Shi, and N. Wang, Lattice BGK model for incompressible NavierStokes equation, *J. Comput. Phys., 165,* 288-306, 2000.
23. Noble, D. R., Lattice Boltzmann study of the interstitial hydrodynamics and dispersion in steady intertial flows in large randomly packed beds, PhD thesis, 1997.

24. Lichtner, P. C., Continuum formulation of multicomponent-multiphase reactive transport, *Reviews in Mineralogy, 34, Reactive Transport in Porous Media,* 1-81, 1996.
25. Lichtner, P. C., Continuum model for simultaneous chemical reactions and mass transport in hydrothermal systems, *Geochimica et Cosmochimica ACTA, 49,* 779-800, 1985.
26. Lu G. P., D. J. DePaolo, Q. Kang, and D. Zhang, Lattice Boltzmann simulation of snow crystal growth in clouds, *J. Geophy. Res.,* in press, 2008.
27. Willingham, T. W., C. J. Werth, and A. J. Valocchi, Evaluation of the Effects of Porous Media Structure on Mixing-Controlled Reactions Using Pore-Scale Modeling and Micromodel Experiments, *Environ. Sci. Technol., 42,* 31853193, 2008.
28. Chou, L., R. M. Garrels, and R. Wollast, Comparative study of the kinetics and mechanisms of dissolution of carbonate minerals. Chem. Geol. 78, 269282, 1989.
29. Gautelier, M., E. H. Oelkers, and J. Schott, An experimental study of dolomite dissolution rates as a function of pH from 0.5 to 5 and temperature from 25 to 80C, Chemical Geology, 157, 1326, 1999.
30. Lichtner, P. C., The quasi-stationary state approximation to coupled mass transport and fluid-rock interaction in a porous medium, Geochim. Cosmochim. Acta, 52, 143-165, 1988.
31. Lichtner, P. C., FLOTRAN user's guide, Los Alamos National Laboratory report, Los Alamos, NM, 1999.

Table 1 Porous media properties.

Structure	Particle size m^2	Porosity	Specific surface area m^{-1}	Permeability m^2
small circles (geo1)	6.61×10^{-8}	0.42	1.38×10^4	8.58×10^{-11}
large circles (geo2)	2.66×10^{-7}	0.42	6.9×10^3	3.38×10^{-10}
horizontal ellipses (geo3)	6.66×10^{-8}	0.42	1.52×10^4	1.02×10^{-10}
vertical ellipses (geo4)	6.66×10^{-8}	0.42	1.52×10^4	3.20×10^{-11}

Table 2 Kinetic rate parameters for dolomite from Gautelier et al. [29].

T [°C]	k[mol cm^{-2}s^{-1}]	n
25°C	9.82×10^{-8}	0.63
50°C	5.13×10^{-7}	0.73
80°C	1.77×10^{-6}	0.80

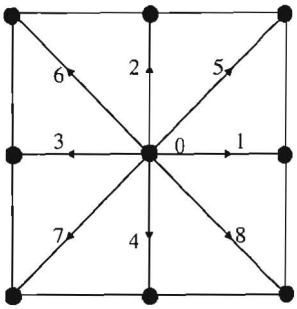

Fig. 1 Schematic illustration of a D2Q9 lattice.

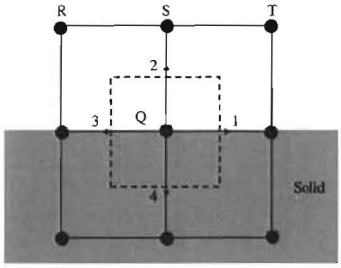

Fig. 2 Schematic illustration of a D2Q4 lattice at a wall node.

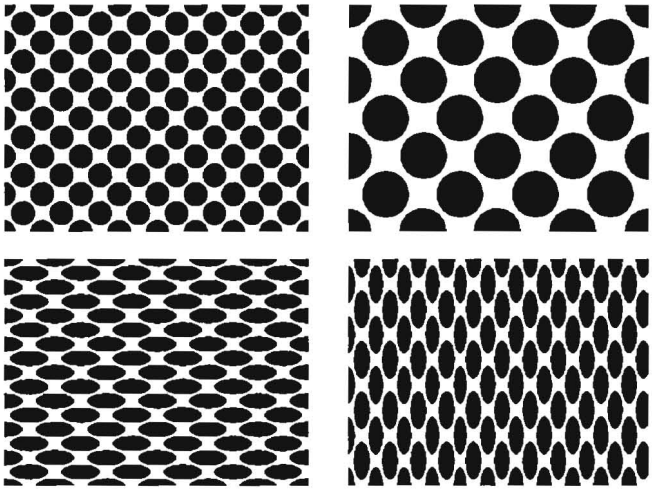

Fig. 3 Porous media structures used in the simulations.

Fig. 4 A representative elemental volume for the periodic array of small circles.

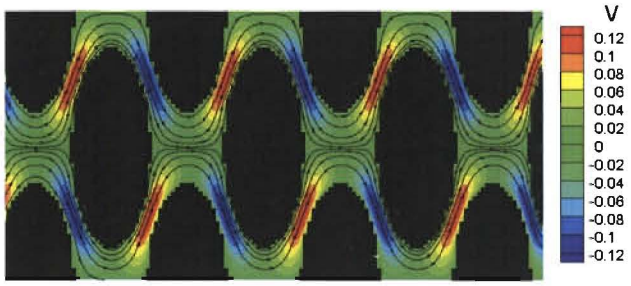

Fig. 5 Velocity field (stream lines and contours of vertical velocity) predicted by the LB model for the vertical ellipse porous medium.

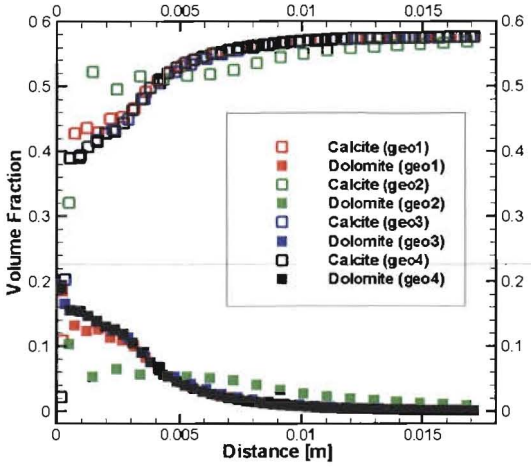

Fig. 6 Distribution of volume-averaged (over an REV) volume fraction of calcite and dolomite along the x-direction at time=9500 seconds and temperature=25°C.

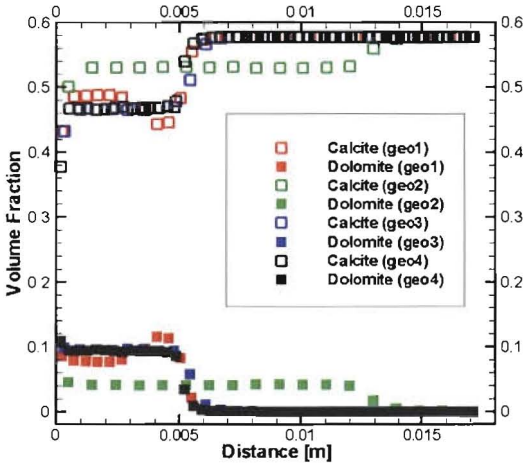

Fig. 7 Distribution of volume-averaged (over an REV) volume fraction of calcite and dolomite along the x-direction at time=9500 seconds and temperature=80°C.

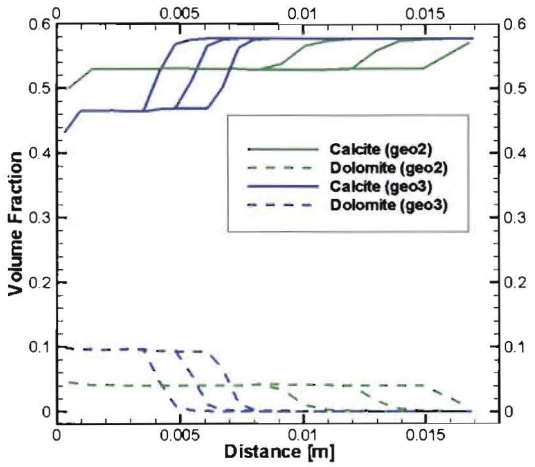

Fig. 8 Distribution of volume-averaged (over an REV) volume fraction of calcite and dolomite along the x-direction at temperature=80°C and time=7000 (left), 9500 (middle), and 12000 (right) seconds.

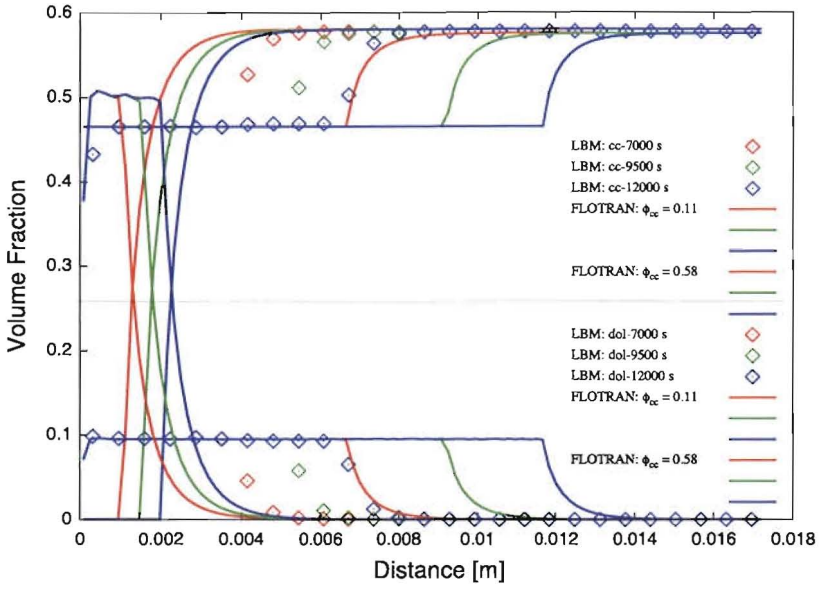

Fig. 9 Continuum scale and LB simulation results of calcite and dolomite volume fraction for horizontal ellipse structure at temperature=80°C and time=7000, 9500, and 12000 seconds. Solid lines at the left and right correspond to a reactive calcite volume fraction of 0.58 and 0.11, respectively, in the continuum scale simulations.

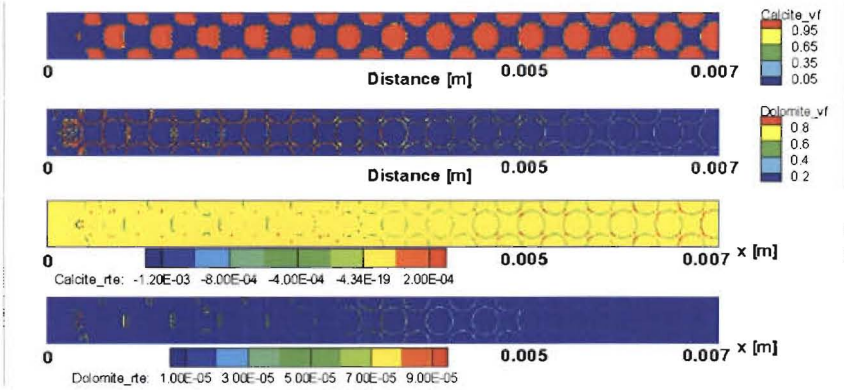

Fig. 10 Spacial distribution of volume fraction and reaction rate of calcite and dolomite for the small circle porous medium at time=9500 seconds and temperature=25°C.

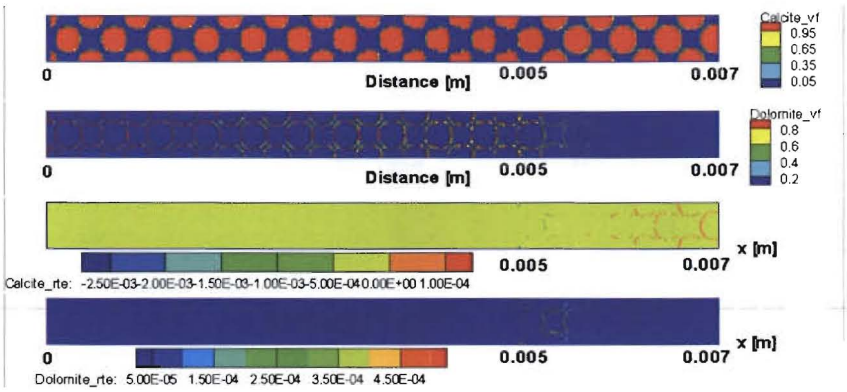

Fig. 11 Spacial distribution of volume fraction and reaction rate of calcite and dolomite for the small circle porous medium at time=9500 seconds and temperature=80°C.

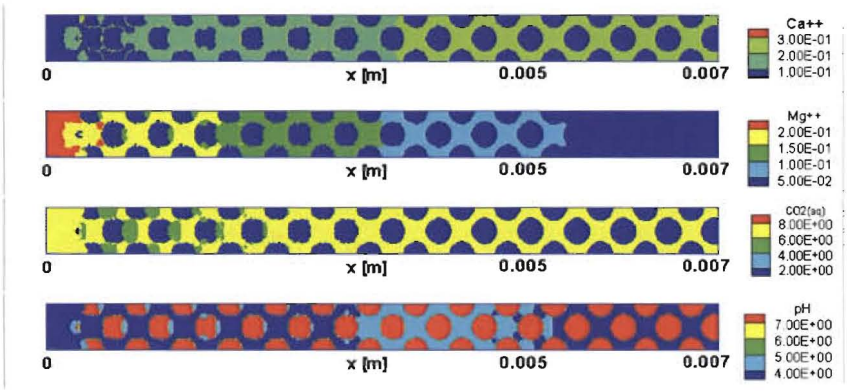

Fig. 12 Concentration distribution of aqueous species for the small circle porous medium at time=9500 seconds and temperature=25°C.

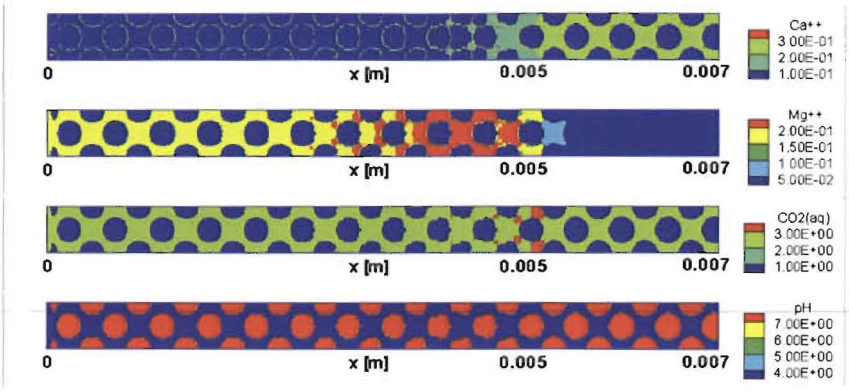

Fig. 13 Concentration distribution of aqueous species for the small circle porous medium at time=9500 seconds and temperature=80°C.